Networks of Coupled Rotators: Relationship between Structures and Internal Dynamics in Metal-Binding Proteins. Applications to *apo-* and *holo-*Calbindin

Anne Dhulesia, Daniel Abergel,* and Geoffrey Bodenhausen

Contribution from the Département de Chimie, Ecole Normale Supérieure, 24, rue Lhomond, 75231 Paris Cedex 05, France

Received October 17, 2006; E-mail: daniel.abergel@ens.fr

Abstract: This article presents an analysis of the internal dynamics of the Ca^{2+}-binding protein calbindin, based on the Networks of Coupled Rotators (NCRs) introduced recently. Several fundamental and practical issues raised by this approach are investigated. The roles of various parameters of the model are examined. The NCR model is shown to account for the modifications of the internal dynamics upon Ca^{2+} binding by calbindin. Two alternative strategies to estimate local internal effective correlation times of the protein are proposed, which offer good agreement between predictions and experiment.

The ability of biological macromolecules such as proteins and nucleic acids to sustain extensive internal motions is believed to be essential to their function. Thus, beyond well-established "structure−activity" relationships, there is increasing evidence that internal mobility of macromolecules plays an important role in biological function and activity.[1] It is tempting to try to establish links between structure and mobility. This problem has been tackled in various ways, mainly by normal-mode analysis (NMA) of atomic motions described by sophisticated[2] or simplified potentials.[3] NMA offers a useful analytical tool that is particularly well suited to rationalize *B*-factors in X-ray diffraction studies. The NMA approach, which is based on a harmonic motional approximation, allows one to calculate atomic mean-square displacements (AMSDs) of all atoms in a protein. Internal motions can be studied experimentally by measuring longitudinal and transverse relaxation rates of ^{15}N nuclei by nuclear magnetic resonance (NMR). Using a model-free approach,[4,5] one can extract a generalized order parameter S_{ii}^2 and an effective internal correlation time τ_{ie} for all vectors $\mathbf{u}(N_iH_i^N)$ and, by extension, for all amide planes $i = 1 \dots N$ in a protein with *N* residues.

Rationalizing local variations of order parameters S_{ii}^2 in terms of a limited set of dynamic parameters is of both fundamental and practical relevance. Recently, we have introduced a simple analytical model for predicting NMR order parameters, based on the dynamics of a network of coupled rotators (NCR).[6,7] This model is particularly well suited for the study of NMR relaxation rates, which are sensitive to the fluctuations of the *orientations* of vectors and tensors that describe magnetic dipole−dipole or anisotropic chemical shift interactions, rather than to the

positions of atoms, as in X-ray diffraction. Indeed, the NCR model describes the dynamics of an ensemble of rotators undergoing diffusion in a phenomenological potential that represents many physical interactions (electrostatic, van der Waals, etc.). This potential is comprised of pairwise coupling potentials that depend only on the deviation from equilibrium of the angle between two interaction vectors. The interaction vectors involved in the description of backbone dynamics may be chosen among a set of internuclear vectors, collected in "vector types" such as $\mathbf{u}(N_iH_i^N)$, $\mathbf{u}(C'_iO_i)$, $\mathbf{u}(C'_iC_i^\alpha)$ with $i = 1, \dots N$. This model shares a common feature with the approach of Haliloglu and Bahar[8] in that the geometric constraints of the motions are determined by the structure. This may represent a limitation of both models. However, despite its simplicity, the NCR approach can predict generalized order parameters S_{ii}^2 and effective internal correlation times τ_{ie} for each residue *i* that agree remarkably well with parameters extracted from experimental relaxation rates.[6]

Several questions regarding this model remain to be investigated. In particular, the way the parameters that define the pairwise potentials influence the dynamic predictions should be clarified. Does the NCR model also allow one to take into account *inter*molecular interactions, such as those between a protein and various charged or neutral ligands, substrates, or cofactors? How do NCR predictions of internal correlation times compare with those extracted from NMR relaxation rates by model-free analysis? Moreover, how does the NCR model compare with NMA? It may not be possible to give definite answers to such broad questions. It is instructive, however, to address these questions in the context of a particular example, in order to identify trends that may be of general value. In this paper, we focus on the calcium-binding protein calbindin. Predictions of the internal dynamics of the Ca^{2+}-free (*apo*) and Ca^{2+}-loaded (*holo*) forms of calbindin obtained by the NCR

(1) Jarymowicz, V. A.; Stone, M. J. *Chem. Rev.* **2006**, *106*, 1624.
(2) Levitt, M. H.; Sander, C.; Stern, P. S. *J. Mol. Biol.* **1985**, *181*, 423.
(3) Tirion, M. *Phys. Rev. Lett.* **1997**, *77*, 1905.
(4) Lipari, G.; Szabo, A. *J. Am. Chem. Soc.* **1982**, *104*, 4546.
(5) Lipari, G.; Szabo, A. *J. Am. Chem. Soc.* **1982**, *104*, 4559.
(6) Abergel, D.; Bodenhausen, G. *J. Chem. Phys.* **2005**, *123*, 204901.
(7) Abergel, D.; Bodenhausen, G. *J. Chem. Phys.* **2004**, *121*, 761.

(8) Haliloglu, T.; Bahar, I. *Proteins: Struct., Funct., Genet.* **1999**, *37*, 654.

model will be compared with experimental observations of NMR relaxation rates[9,10] and with experimental and calculated *B*-factors.[11] Finally, we introduce a new strategy for predicting local effective internal correlation times. This approach will be illustrated by applications to calbindin and compared with the usual model-free approach.

The Model

In the NCR approach, each member of an ensemble of internuclear vectors $\mathbf{u}_i$ is assumed to undergo a diffusional "wobbling" motion in a potential. This potential results from a superposition of terms U_{ij}, each of which reflects the coupling between a pair of vectors $\mathbf{u}_i$ and $\mathbf{u}_j$. Thus the angle $\theta_{ij}(t)$ subtended by these two vectors fluctuates about an equilibrium value θ_{0ij}, which is defined by the (average) equilibrium structure of the protein. For small fluctuations, for which $|\theta_{ij} - \theta_{0ij}| < \pi/2$, one may postulate:

$$U_{ij} = -\rho_i \rho_j \kappa_0 kT P_2(\cos(\theta_{ij} - \theta_{0ij})) \tag{1}$$

where k is the Boltzmann constant, T, the temperature, κ_0, an adjustable parameter that is common to all pairs of vectors, and $P_2(x) = (3x^2 - 1)/2$, the second-rank Legendre polynomial. The potential U_{ij} reaches a minimum for $\theta_{ij} = \theta_{0ij}$ and thus tends to restore the instantaneous angle $\theta_{ij}(t)$ between the vectors $\mathbf{u}_i$ and $\mathbf{u}_j$ to its equilibrium value θ_{0ij}. Moreover, each pair potential U_{ij} is proportional to the product $\rho_i \rho_j$, where ρ_i and ρ_j are the *local densities* in the vicinity of the "reference atoms" (see below) of the coupled vectors. Indeed, the local packing in the neighborhood of the coupled vectors is known to influence their dynamics.[6,12,13] We define the overall potential U as the superposition of all pairwise potentials U_{ij}:

$$U = \Sigma_{i<j} U_{ij} \tag{2}$$

The dynamics of each vector $\mathbf{u}_i$ in the molecule thus depends on all N coupled vectors $\mathbf{u}_j$, with $j = 1,..., N$, $j \neq i$. Although there is no explicit distance dependence in the interacting potential, it is introduced implicitly by retaining only interactions involving atoms separated by less than a cutoff distance R_c^{max}. This point will be further examined below. The choice of the vectors that together constitute the NCR network, and therefore contribute to the potential, depends to some extent on the purpose of the study. When internal protein motions are probed by ^{15}N relaxation, the vectors $\mathbf{u}(N_i H_i^N)$ must obviously be included in the network. In many cases, it is advisable to incorporate additional types of vectors that are associated with backbone or side-chain atoms. For example, the set of "backbone vectors" may include the vector types $\mathbf{u}(C'_i O_i)$, $\mathbf{u}(C_i^\alpha H_i^\alpha)$, and $\mathbf{u}(C'_i C_i^\alpha)$, and the "side-chain vectors" may comprise $\mathbf{u}(C_i^\alpha C_i^\beta)$ and $\mathbf{u}(C_i^\alpha T_i)$, where T_i represents a heavy atom at the end of a side chain. As detailed below, several combinations, including up to three vector types, were used in this work. If one changes the number of vector types used in the model, a recalibration of the parameter κ_0 is necessary.

Since proteins are densely packed molecules, the motions of most of the vectors $\mathbf{u}_i$ are restricted, and their amplitudes are necessarily limited. In this context, we have shown that the following form of the pairwise potentials gives a satisfactory description:

$$U_{ij} = -\left(\frac{1}{2}\right)\kappa_0 kT \rho_i \rho_j [u_{ix}, u_{iy}, u_{jx}, u_{jy}] \; \mathbf{H}[u_{ix}, u_{iy}, u_{jx}, u_{jy}]^t \tag{3}$$

where the coefficients of the matrix $\mathbf{H}$ relate the equilibrium polar angles (θ_{i0}, ϕ_{i0}) and (θ_{j0}, ϕ_{j0}) of the vectors $\langle\mathbf{u}_i\rangle$ and $\langle\mathbf{u}_j\rangle$, while the components u_{xi} and u_{yi} of $\mathbf{u}_i$ are given in a local molecule-fixed Cartesian frame $R_i = (\mathbf{a}_i, \mathbf{b}_i, \mathbf{c}_i)$, such that $\mathbf{c}_i = \langle\mathbf{u}_i\rangle$. Similar relationships hold for $\mathbf{u}_j$. Explicit expressions for the coefficients of the matrix $\mathbf{H}$ are given in earlier work.[6]

Ming and Brüschweiler[14] recently introduced pairwise potentials that tend to restore the angles between pairs of NH vectors to their equilibrium values. Neighboring atoms contribute as in their earlier contact model.[13] Despite different functional forms of the potentials, the model of Ming and Brüschweiler and ours bear some similarities, with structure-based potentials where atomic packing plays a key role. However, the approach presented by Ming and Brüschweiler does not provide a means of calculating effective correlation times, since it does not incorporate any equations of motion. However, the time evolution can be retrieved through molecular dynamics using the Reorientational Eigenmode Dynamics (RED) of Prompers and Brüschweiler.[15]

In the NCR model, the vectors are diffusing or "wobbling" in the potential U and are driven by stochastic Langevin forces. Averages that are required for the calculation of NMR relaxation rates, such as correlation functions and generalized order parameters, can be determined by solving the rotational Langevin equations.[16] Thus the autocorrelation function $C_{ii}(t)$ that describes the fluctuations of a vector $\mathbf{u}_i$ is

$$C_{ii}(t) = \frac{1}{5}\langle P_2(\mathbf{u}_i(t) \cdot \mathbf{u}_i(0))\rangle \tag{4}$$

Here, $P_2(x) = \frac{1}{2}(3x^2 - 1)$ is again the second-rank Legendre polynomial. For molecules undergoing isotropic global rotational diffusion, where global and internal motions can be considered to be statistically independent,[4,5] each local correlation function $C_{ii}(t)$ can be factorized

$$C_{ii}(t) = C^0(t) \, C_{ii}^I(t) \tag{5}$$

where $C^0(t)$ and $C_{ii}^I(t)$ are the correlation functions for the global and internal motions. For a vector $\mathbf{u}_i$, the latter can be written:[17]

$$C_{ii}^I(t) = \sum_{m=-2}^{2} \langle D_{m0}^{(2)*}(\Omega_i(0)) \, D_{m0}^{(2)}(\Omega_i(t))\rangle \tag{6}$$

where the Euler angles $\Omega_i = (\theta_i, \phi_i)$ describe the fluctuating orientation of the vector $\mathbf{u}_i$ with respect to a reference frame rigidly attached to the molecule. Making the assumption of small amplitude motions for the vectors $\mathbf{u}_i$, the order parameter S_{ii}^2

(9) Akke, M.; Skelton, N. J.; Kördel, J.; Palmer, A. G., III; Chazin, W. J. *Biochemistry* **1993**, *32*, 9832.
(10) Kordel, J.; Skelton, N. J.; Akke, M.; Palmer, A. G. I.; Chazin, W. J. *Biochemistry* **1992**, *31*, 4856.
(11) Svensson, L. A.; Thulin, E.; Forsen, S. *J. Mol. Biol.* **1992**, *223*, 601.
(12) Halle, B. *Proc. Natl. Acad. Sci. U.S.A.* **2002**, *99*, 1275.
(13) Zhang, F.; Bruschweiler, R. *J. Am. Chem. Soc.* **2002**, *124*, 12654.

(14) Ming, D.; Bruschweiler, R. *Biophys. J.* **2006**, *90*, 3382.
(15) Prompers, J. J.; Bruschweiler, R. *J. Am. Chem. Soc.* **2001**, *123*, 7305.
(16) Coffey, W. T.; Kalmykov, Y. P.; Waldron, J. T. *The Langevin Equation*; World Scientific: Singapore, 1996.
(17) Daragan, V. A.; Mayo, K. H. *Progr. NMR Spectrosc.* **1997**, *32*, 63.

can be expressed in the local frame R_i as[6,18]

$$S_{ii}^2 = \lim_{t \to \infty} C_{ii}^I(t) \approx 1 - 3[\langle u_{ix}^2 \rangle^{eq} + \langle u_{iy}^2 \rangle^{eq}] \qquad (7)$$

With the above approximations, it is possible to derive a set of ordinary differential equations for the averages involved in eq 7. Thus the network of coupled rotators allows one to predict both the local order parameters S_{ii}^2 and the internal autocorrelation functions $C_{ii}^I(t)$, both of which can be compared with those determined from NMR relaxation experiments.

Finding a simple approximation to $C_{ii}^I(t)$ represents an important issue in NMR relaxation studies. A common approach is to use a monoexponentially decaying function with a time constant τ_{ie}, which is known as the effective correlation time of the local motion. The quantity τ_{ie} can be defined as the integral of the $C_{ii}^I(t)$ that decays to zero:[4]

$$\tau_{ie} = \int_0^\infty \frac{C_{ii}^I(t) - S_{ii}^2}{1 - S_{ii}^2} \, \mathrm{d}t \qquad (8)$$

This is consistent with the usual definition. Therefore, the correlation function $C_{ii}^I(t)$ is simply

$$C_{ii}^I(t) = S_{ii}^2 + (1 - S_{ii}^2) \, \mathrm{e}^{-t/\tau_{ie}} \qquad (9)$$

An alternative definition of the effective correlation time[16] is based on the initial slope of the correlation function $C_{ii}^I(t)$:

$$\tilde{\tau}_{ie} = \frac{S_{ii}^2 - C_{ii}^I(0)}{\dfrac{\mathrm{d}}{\mathrm{d}t} C_{ii}^I(t)|_{t=0}} \qquad (10)$$

Since this definition emphasizes the behavior of the correlation function at the origin, it may be better suited to describe faster internal dynamics. Of course, in the case of an exact monoexponential correlation function as given by eq 9, both definitions are identical. The ability of the NCR model to predict effective correlation times found by experiment will be discussed below, along with a comparison between the two alternative definitions of the correlation times.

The Networks

Construction of NCRs for *apo*- and *holo*-Calbindin. The present work is primarily concerned with the prediction of order parameters and effective correlation times that can be obtained from experimental ^{15}N relaxation rates, which are determined by the fluctuations of $\mathbf{u}(N_iH_i^N)$ vectors. This requires the inclusion of all $\mathbf{u}(N_iH_i^N)$ vectors in the NCR, i.e., one for each residue, except for prolines, where $\mathbf{u}(N_iH_i^N)$ must be replaced by $\mathbf{u}(N_iC_i^\delta)$. Other types of vectors, such as $\mathbf{u}(C_i'O_i)$ and $\mathbf{u}(C_i^\alpha H_i^\alpha)$ (two such vectors for glycines), can be further incorporated into the network. In order to study the changes in internal dynamics of calbindin induced by Ca^{2+} binding, we also introduced $\mathbf{u}(CaO_i)$ vectors parallel to the Ca–O bonds that are formed when the metal ions bind to the protein. Indeed, calbindin possesses two Ca^{2+} binding sites with a characteristic EF-hand motif. In *holo*-calbindin, both Ca^{2+} ions are bound to oxygen atoms belonging to various backbone carbonyl C=O groups and to carboxylic groups of side chains.[11] Thus, six
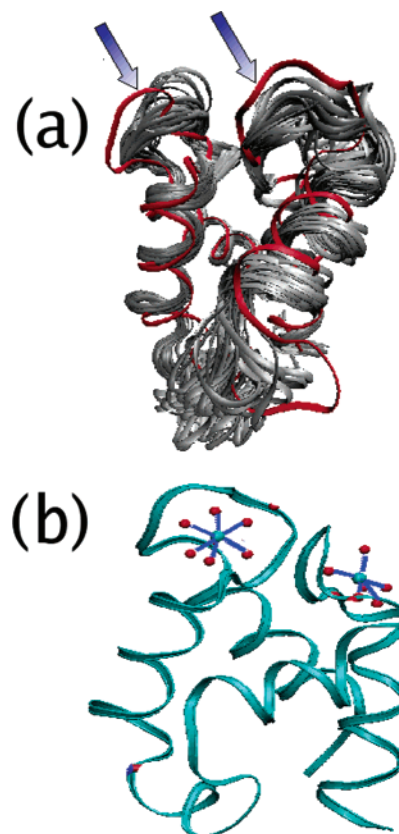
Figure 1. (a) The family of 33 structures of *apo*-calbindin (PDB entry 1CLB) obtained by NMR (gray) is superimposed with the X-ray structure (red) of *holo*-calbindin (PDB entry 4ICB). Regions where the structure is not well-defined correspond to the Ca^{2+} binding sites (indicated by blue arrows) and to the linker between the two EF-hands (in the lower-right region of the figure). (b) The X-ray structure of *holo*-calbindin (PDB entry 4ICB) shows the two Ca^{2+} ions (blue) connected to their binding oxygen atoms (red balls) by vectors included in the network of coupled rotators (blue arrows).

$\mathbf{u}(CaO_i)$ vectors were introduced for each binding site, as shown in Figure 1b. For the $\mathbf{u}(CaO_i)$ vectors, the local distances were determined for spheres centered on the oxygen atoms O_i.

Calbindin Structures Used for the Calculations. The structures of *apo*-calbindin[19] (entry 1CLB in the PDB, 33 structures) and *holo*-calbindin[20,21] (entry 1B1G in the PDB, 10 structures), which have been determined by NMR, were used for the NCR calculations. The X-ray structure of *holo*-calbindin[11] (entry 4ICB in the PDB) could also serve as a basis for NCR calculations: indeed, the hydrogen atoms were positioned using the Hbuild routine of the CHARMM program,[22] with the equilibrium geometric parameters of CHARMM22, thus allowing to define the $\mathbf{u}(N_iH_i^N)$ vectors required for the NCR calculations.

Unfortunately, the X-ray structure of *apo*-calbindin has not been determined to the best of our knowledge. It was nevertheless interesting to predict the dynamics of calbindin from a "fictitious" *apo* X-ray structure, which was obtained simply by removing the Ca^{2+} ions from the *holo* X-ray structure. Of course, this implies that some structural changes that might occur upon

(18) Daragan, V. A.; Mayo, K. H. *J. Phys. Chem. B* **1999**, *103*, 6829.

(19) Skelton, N. J.; Kordel, J.; Chazin, W. J. *J. Mol. Biol.* **1995**, *249*, 441.
(20) Kordel, J.; Skelton, N. J.; Akke, M.; Chazin, W. J. *J. Mol. Biol.* **1993**, *231*, 711734.
(21) Kordel, J.; Pearlman, D. A.; Chazin, W. J. *J. Biomol. NMR* **1997**, *10*, 231.
(22) Brooks, B.; Bruccoleri, R. E.; Olafson, B. D.; States, D. J.; Swaminathan, S.; Karplus, M. *J. Comp. Chem.* **1983**, *4*, 187.
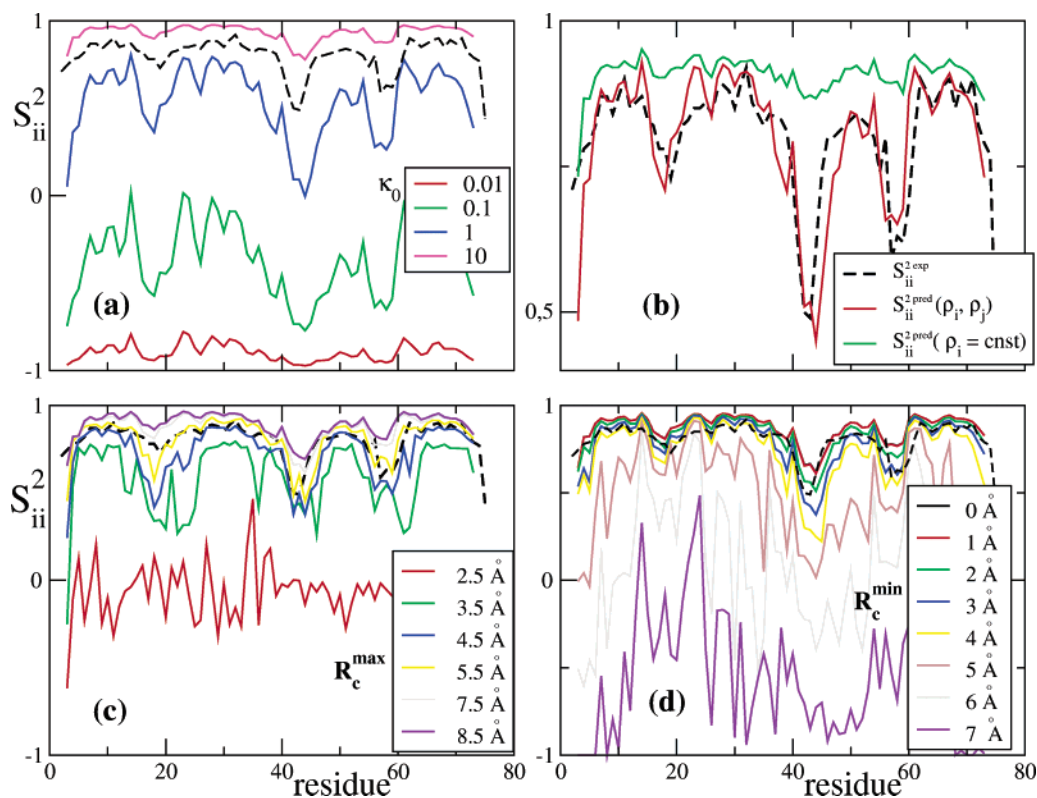
Figure 2. Comparison of order parameters $S_{ii}^{2(pred)}$ predicted by our NCR approach (color code) with $S_{ii}^{2(exp)}$ (black dashed lines) derived from ^{15}N relaxation studies of *apo*-calbindin. (a) Effect of the scaling factor κ_0: for small values of κ_0, there is no correlation between experimental and theoretical profiles, whereas for large values of κ_0 all predicted order parameters tend to cluster to 1. (b) Comparison of predictions for a constant local density ρ_i with predictions obtained using the densities calculated from the NMR structure of the protein. (c) Effect of the cutoff distance R_c^{max} with $R_c^{min} = 0$ Å. (d) Variation of R_c^{min} with $R_c^{max} = 7.5$ Å.

Ca^{2+} release would be overlooked. However, the comparison in Figure 1 of the 33 NMR-derived structures of *apo*-calbindin with the unique X-ray structure of *holo*-calbindin shows that they are all quite similar, and their dispersion may reflect the heterogeneity of the native state.[23] Therefore, performing NCR calculations for the *apo* case using the fictitious X-ray structure appears justified. Thus, the NCR of *apo*-calbindin was obtained from its *holo* counterpart simply by removing all **u**(CaO$_i$) vectors.

Effect of Model Parameters on Predictions: Critical Parameters. The parameter κ_0 of eq 1 defines the weight of the coupling potential relative to the diffusion term in the Langevin equations.[6,7] On the one hand, if κ_0 were too small, diffusion would be dominant and the bond vectors would diffuse almost freely. However, in such a case, the assumption of small amplitude motions is violated and the NCR model should not be used. This explains the curves in Figure 2a obtained for small values of $\kappa_0 = 0.01$ and 0.1 which present $S_{ii}^{2(pred)}$ profiles that are hardly correlated with the experimental $S_{ii}^{2(exp)}$. On the other hand, for a large value of $\kappa_0 = 10$ in Figure 2a, the coupling potential dominates the diffusion process by far: the network is highly rigid, and the order parameters $S_{ii}^{2(pred)}$ are consistently close to 1. They nevertheless present a profile that is still similar to the experimental one. Interestingly, for κ_0 values above some threshold ($\kappa_0 = 1$ in Figure 2a), the linear and rank-order correlation coefficients between predicted and experimental order parameters $S_{ii}^{2(pred)}$ and $S_{ii}^{2(exp)}$ do not vary signifi-

cantly, although $S_{ii}^{2(pred)}$ values steadily increase with κ_0. This parameter thus acts as a scaling factor for the predicted order parameters.

Taking the local density into account improves the agreement between $S_{ii}^{2(pred)}$ and $S_{ii}^{2(exp)}$, as shown in Figure 2b. This should be related to the well-known influence of "packing" in proteins, which has been recognized as a critical factor of atomic mobility.[12,13] However, the profiles in Figure 2b also show that even if variations in local densities are ignored when defining the pairwise potentials, the predicted order parameters bear some similarity with experimental values. This points to an additional fundamental geometric factor that is at the heart of the NCR model, namely the importance of the relative equilibrium orientations of the vectors $\langle \mathbf{u}_i \rangle$ in the network, which are embodied in the pairwise potentials through the coefficients in eq 3. The definition of the network influences the quality of the predictions of both S_{ii}^2 and τ_{ie}. In this respect, two factors are of particular importance: the type of vectors included in the NCR and the spatial extent of the coupling within the network. As explained above, $\mathbf{u}(N_iH_i^N)$ vectors were included in the NCR since they provide a direct link with ^{15}N relaxation, which depends on the fluctuations of $\mathbf{u}(N_iH_i^N)$ vectors. Furthermore, various combinations of up to three of the five types of vectors $\mathbf{u}(N_iH_i^N)$, $\mathbf{u}(C'_iO_i)$, $\mathbf{u}(C_i^\alpha H_i^\alpha)$, $\mathbf{u}(C'_iC_i^\alpha)$, and $\mathbf{u}(C_i^\alpha T_i)$ were tested to build the networks. For calculations on *holo*-calbindin, the networks were supplemented by $\mathbf{u}(CaO_i)$ vectors. Interestingly, the $S_{ii}^{2(pred)}$ order parameters were improved by adding a second vector type, but adding a third type of vector did not seem to improve the predictions further.

(23) Best, R. B.; Lindorff-Larsen, K.; DePristo, M. A.; Vendruscolo, M. *Proc. Natl. Acad. Sci. U.S.A.* **2006**, *103*, 10901.

Table 1. Linear and Spearman Rank-Order Correlation Coefficients ρ_l and ρ_s Resulting from a Comparison of NCR-Predicted Order Parameters $S_{ii}^{2(pred)}$ with $S_{ii}^{2(exp)}$ Derived from ^{15}N Relaxation Studies of *apo*- and *holo*-Calbindin[a]

NCR predictions based on NMR or X-ray structures	ρ_l	ρ_s
apo (NMR)	0.74 ± 0.08	0.78 ± 0.03
apo ("fictitious" X-ray)	0.59	0.78
holo (NMR)	0.71 ± 0.1	0.49 ± 0.03
holo (X-ray)	0.81	0.52

[a] In the former case, the NCR network includes $\mathbf{u}(C'_iO_i)$ and $\mathbf{u}(N_iH_i^N)$ vectors only; in the latter, it also comprises $\mathbf{u}(CaO_i)$ vectors.

In order to obtain an NCR that best reproduces the dynamics of the protein, and to speed up computations, it is useful to assume that couplings between vectors can be neglected beyond a cutoff distance R_c^{max}. This represents a crude distance dependence in our definition of the potential, expressing the intuitive view that the farther the atoms, the weaker the coupling. In order to implement this assumption, the *reference atoms* of the vectors $\mathbf{u}_i$ were defined by convention as the backbone atoms N_i and C_i^α for $\mathbf{u}(N_iH_i^N)$, $\mathbf{u}(C_i^\alpha H_i^\alpha)$, and $\mathbf{u}(C_i^\alpha T_i)$, as the carbonyl atoms C'_i for $\mathbf{u}(C'_iO_i)$ and as the oxygen O_i atoms for $\mathbf{u}(CaO_i)$. For a distance R_{ij} between reference atoms belonging to two vectors $\mathbf{u}_i$ and $\mathbf{u}_j$ such that $R_{ij} > R_c^{max}$, the coupling was neglected. The densities ρ_i were calculated for spheres centered on these reference atoms by counting the total number of neighbors within a sphere of radius R_c^{max}. Calculations were performed for cutoff distances ranging from $R_c^{max} = 1.5$ Å, typical of a chemical bond length, to $R_c^{max} = 10.5$ Å. The correlations between predicted and experimental S_{ii}^2 and τ_{ie} values steadily improve with R_c^{max} increasing up to about 7 Å and then slightly decrease. This suggests that, for excessively large cutoff distances, too many vectors are included in the definition of the network, resulting in a potential that tends to be almost isotropic and leading to an excessive uniformity of the vector dynamics across the entire protein. Interestingly, the low S_{ii}^2 values that are characteristic of flexible regions of calbindin could be predicted with thresholds as small as $R_c^{max} = 4.5$ Å. The best correlations between predicted and experimental S_{ii}^2 and τ_{ie} were obtained in the range 5.5 Å $< R_c^{max} < 7.5$ Å, in agreement with previous studies.[12,24] A cutoff distance $R_c^{max} = 7.5$ Å allowed the characterization of many important protein properties.

Finally, the influence of atoms located in close vicinity of the reference atoms was considered. To do so, the network vectors were selected and the densities were calculated using a window with both lower and upper cutoffs, so as to include only neighbors with a distance to the reference atom $R_c^{min} < R < R_c^{max}$. For simplicity, the upper limit was set to $R_c^{max} = 7.5$ Å, while R_c^{min} was varied from $0 < R_c^{min} < 7$ Å in steps of 1 Å. Interestingly, the S_{ii}^2 profiles are not greatly affected for values of R_c^{min} below 4 Å. This is in agreement with an observation by Halle[12] and supports the idea that the effect of the close neighborhood of backbone atoms is rather uniform, so that it does not contribute much to variations of the order parameter along the protein. In contrast, more distant atoms reflect the heterogeneity of the protein structure, which seems to explain the specificity of the protein dynamics.

With a single set of parameters ($R_c^{max} = 7.5$ Å and $\kappa_0 = 2.5$) and an NCR comprising all $\mathbf{u}(N_iH_i^N)$ and $\mathbf{u}(C'_iO_i)$ vectors, as well as $\mathbf{u}(CaO_i)$ for the *holo* case, the agreement between
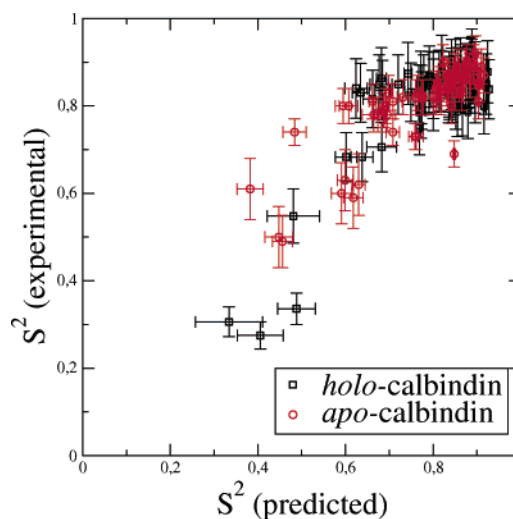
Figure 3. Correlation between predicted and experimental order parameters in *apo*-calbindin (red) and *holo*-calbindin (black). Horizontal error bars correspond to the standard deviation of the order parameters calculated for $M = 33$ (*apo*) and $M = 10$ (*holo*) NMR structures.

predicted and experimental S_{ii}^2 values in calbindin, measured by either linear or Spearman correlation coefficients,[25] is quite remarkable (see Table 1). Unless otherwise stated, the same set of parameters and vector types will be used throughout this work. However, it is important to note that the parameters (R_c^{max}, κ_0) were determined specifically for calbindin. We do not claim to have determined a universal set of parameters that would be valid for arbitrary proteins, although we believe to have identified some important trends and features of the NCR model, based on our calbindin study.

Predictions for *apo*-Calbindin

Order Parameters. Order parameters predicted by the NCR approach based on the NMR structure of calbindin in the *apo* form[19] were compared with NMR-derived order parameters.[9] Results are shown in Figure 4a. From the set of $M = 33$ structures deposited in the protein data bank (PDB), an average order parameter and its associated standard deviation were predicted for each residue i. Thus, the dispersion of the predicted order parameters originates only from the variations in the PDB structures. The agreement between predicted and experimental order parameters is attested by a strong correlation between the two sets of values. The average value $\langle\rho\rangle = (1/M)\Sigma_{j=1,M} \rho^{(j)}$, where $\rho^{(j)}$ is the correlation coefficient between the experimental and predicted quantities for the jth element in the ensemble of $j = 1, 2, ..., M$ structures, and the corresponding standard deviation

$$\sigma_\rho = \sqrt{1/M \sum_{j=1,M} (\rho^{(j)} - \langle\rho\rangle)^2}$$

of the correlation coefficients were then computed over the $M = 33$ structures. A correlation plot of predicted versus experimental order parameters is shown in Figure 3. Both the linear correlation coefficient $\langle\rho_l\rangle = 0.74 \pm 0.08$ and the rank-order

(24) Bahar, I.; Jernigan, R. L. *J. Mol. Biol.* **1997**, *266*, 195.
(25) Press, W. H.; Flannery, B. P.; Teukolsky, S. A.; Vetterling, W. T. *Numerical recipes*; Cambridge University Press, 1989.
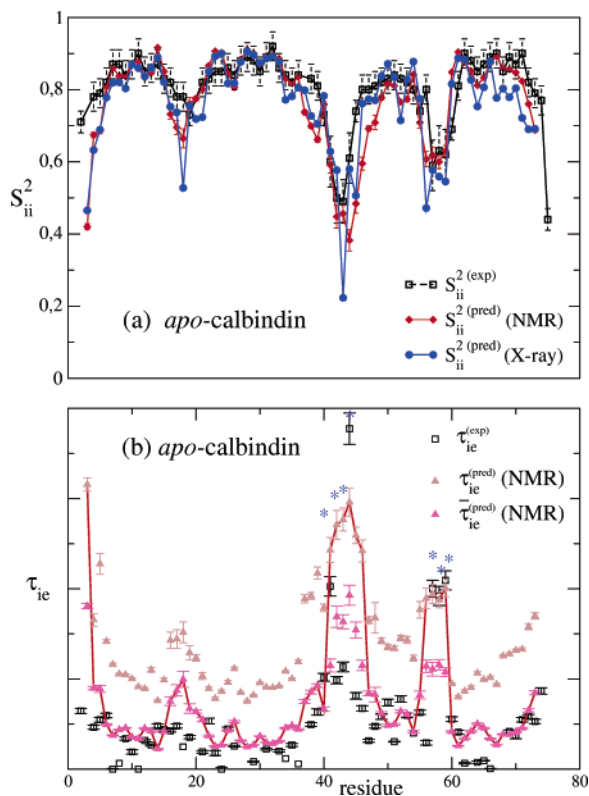
Figure 4. (a) Black open squares: experimentally determined order parameters $S_{ii}^{2(exp)}$ based on ^{15}N relaxation rates. Red diamonds: order parameters $S_{ii}^{2(pred)}$ predicted by the NCR approach, averaged over calculations for all 33 NMR structures of *apo*-calbindin. Error bars indicate the standard deviations; the linear and Spearman correlation coefficients are $\langle\rho_l\rangle = 0.74 \pm 0.08$ and $\langle\rho_s\rangle = 0.78 \pm 0.03$. Blue circles: $S_{ii}^{2(pred)}$ predicted by the NCR method from the X-ray structure. (b) Effective correlation times τ_{ie} (brown triangles) and $\tilde{\tau}_{ie}$ (magenta triangles) calculated with the alternative approaches of eqs 8 and 10 from the set of 33 NMR structures. Values selected according to the heuristic strategy described in the text are connected by a solid red line. Experimentally determined $\tau_{ie}^{(exp)}$ values obtained from a model-free analysis[9] are represented by open black squares. The correlation coefficients were $\rho_l = 0.57 \pm 0.10$ and $\rho_s = 0.65 \pm 0.05$. Calculations were made using $\mathbf{u}(N_iH_i)$ and $\mathbf{u}(C_i'O_i)$ vectors, with $\kappa_0 = 3$ and $R_c^{max} = 7.5$ Å. When the relaxation rates required an extended model-free approach, the residues are marked with blue stars (see text for details).

Spearman coefficient $\langle\rho_s\rangle = 0.78 \pm 0.03$ confirm the agreement between experimental and predicted values.

The two EF-hand loops involved in Ca^{2+} binding, as well as the linker between helices II and III are regions that exhibit more variability within the PDB set. By restricting the calculation of the correlation coefficients to these regions, we obtained $\langle\rho_l\rangle = 0.65 \pm 0.1$ and $\langle\rho_s\rangle = 0.68 \pm 0.06$. These values are somewhat lower than in the remainder of the protein, and have larger standard deviations. This is a consequence of local variations among the PDB structures, and illustrates the dependence of NCR predictions on the structure.

Alternatively, order parameters S_{ii}^2 were predicted from the fictitious X-ray structure of *apo*-calbindin, as explained above. The network was built with the same vectors as in calculations based on the family of 33 NMR structures. Computations yielded $\rho_l = 0.60$ and $\rho_s = 0.78$, which fall within the standard deviations of the correlation coefficients obtained for the NMR structures, suggesting that the fictitious X-ray structure (i.e., with the Ca^{2+} ions removed) is just as suitable as the NMR structures to make dynamic predictions for *apo*-calbindin (see Table 1).

Order parameters were also predicted for *apo*-calbindin by
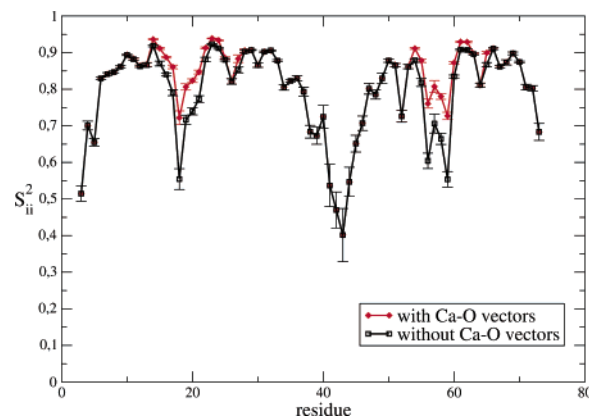
Figure 5. The effect of the insertion of $\mathbf{u}(CaO_i)$ vectors into the NCR on predicted order parameters $S_{ii}^{2(pred)}$ for *holo*-calbindin. Black open squares: NCR defined by $\mathbf{u}(N_iH_i^N)$ and $\mathbf{u}(C_i'O_i)$ vectors only. Red filled diamonds: NCR with incorporation of $\mathbf{u}(CaO_i)$ vectors, which leads to a reduction of the motions near the binding sites.

Ming and Brüschweiler using their reorientational contact-weighted elastic network model (rCENM).[14] Comparable correlation coefficients were obtained. This may be ascribed to the similarities of the two models, both of which depend on the number of neighbors ("contacts") and are based on pairwise potentials.

Effective Correlation Times. The determination of the time-scales of internal motions is an important aspect of protein dynamics. In this respect, the calculation of site-specific effective correlation times τ_{ie} is of much interest, as they can be readily compared with values obtained from NMR relaxation measurements. In the NCR model, each vector $\mathbf{u}_i$ in the network is assumed to undergo isotropic rotational diffusion in the potential defined by eq 3. Thus, the value of the diffusion coefficient D_i of each vector $\mathbf{u}_i$ appearing in the rotational Langevin equations[6] can be thought of as an adjustable parameter of the model. However, for sake of simplicity, one may arbitrarily assign the same diffusion coefficient D to all rotators. Thus, D simply acts as a scaling factor for all time-scales of internal dynamics predicted by the model. This is obviously a very crude approximation, but it has the advantage of keeping the number of adjustable parameters as small as possible.

The τ_{ie} profiles were predicted by NCR using the usual definition eq 8 and compared with experimental effective correlation times obtained from a model-free analysis.[4,5] The results are shown in Figure 4b for *apo*-calbindin.[19] The correlation coefficients between predictions and experiment are $\rho_l = 0.57 \pm 0.10$ and $\rho_s = 0.65 \pm 0.05$. The predictions of internal effective correlation times τ_{ie} and $\tilde{\tau}_{ie}$ computed by the two alternative definitions of eqs 8 and 10 were then compared. Interestingly, both give similar correlations with experimental values, but as expected, τ_{ie} is always larger than $\tilde{\tau}_{ie}$. This is not surprising, since the calculation of τ_{ie} emphasizes contributions to correlation functions at longer times, reflecting slower motions. Besides, it is remarkable that there is no simple scaling between either of the calculated effective correlation times τ_{ie} and $\tilde{\tau}_{ie}$, on the one hand, and the experimental $\tau_{ie}^{(exp)}$, on the other. Adjusting the shorter τ_{ie} to experimental results leads to underestimating τ_{ie} in loop regions, where $\tau_{ie}^{(exp)}$ is longer. Alternatively, fitting τ_{ie} to the latter yields an unreasonable offset of the ensemble of smaller τ_{ie}. These observations suggested that $\tilde{\tau}_{ie}$ and τ_{ie} may be good approximations for fast and slow
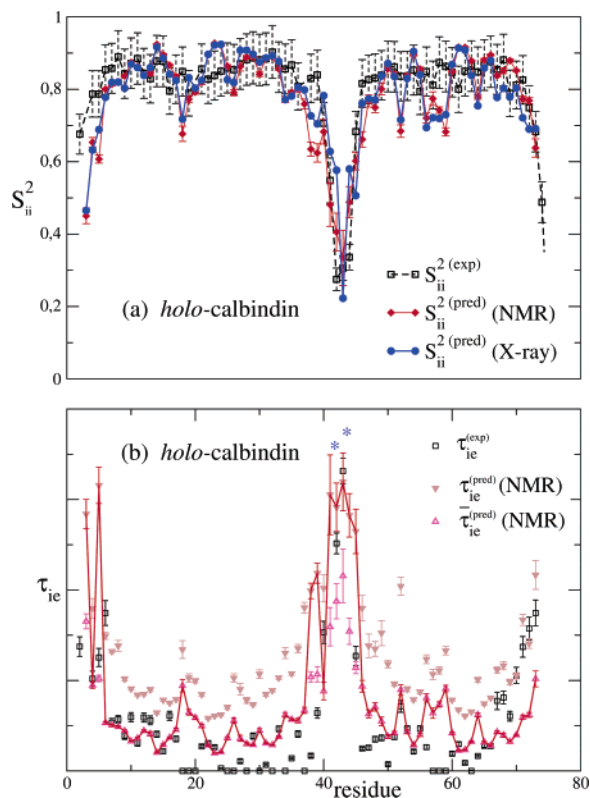
Figure 6. (a) Comparison of order parameters $S_{ii}^{2(pred)}$ predicted by our NCR approach (red and blue symbols) for *holo*-calbindin with $S_{ii}^{2(exp)}$ (open squares) derived from ^{15}N relaxation studies. The correlation coefficients were $\rho_l = 0.71 \pm 0.13$ and $\rho_s = 0.48 \pm 0.03$. (b) Experimental and predicted effective correlation times τ_{ie} and $\tilde{\tau}_{ie}$ calculated with the alternative approaches of eq 8 (open circles) and eq 10 (open squares) with correlation coefficients $\rho_l \approx 0.74$, $\rho_s \approx 0.57$. The network was composed of $\mathbf{u}(N_iH_i^N)$, $\mathbf{u}(C'_iO_i)$ and $\mathbf{u}(CaO_i)$ vectors, with $\kappa_0 = 3$ and $R_c^{max} = 7.5$ Å. The symbols have the same meaning as those in Figure 4.

Table 2. Effect on NCR Predictions of the Incorporation of $\mathbf{u}(CaO_i)$ Vectors for *holo*-Calbindin[a]

NCR predictions	without $\mathbf{u}(CaO_i)$		with $\mathbf{u}(CaO_i)$	
	ρ_l	ρ_s	ρ_l	ρ_s
$S_{ii}^{2(pred)}$ vs $S_{ii}^{2(exp)}$	0.61 ± 0.14	0.51 ± 0.03	0.71 ± 0.13	0.48 ± 0.03
$\tau_{ie}^{(pred)}$ vs $\tau_{ie}^{2(exp)}$	0.63 ± 0.13	0.48 ± 0.08	0.68 ± 0.12	0.55 ± 0.06

[a] Linear and Spearman rank-order correlation coefficients ρ_l and ρ_s resulting from a comparison between predicted and experimental order parameters $S_{ii}^{2(pred)}$ and $S_{ii}^{2(exp)}$ and between predicted and experimental effective correlation times $\tau_{ie}^{(pred)}$ and $\tau_{ie}^{(exp)}$. Calculations are based on the family of 10 NMR structures.

internal motions, respectively. Thus, the predicted τ_{ie} values were separated into two categories, corresponding to *short* and *long* effective correlation times, respectively. In practice, values of τ_{ie} that were closer than a standard deviation to the average $\langle \tau_{ie} \rangle = (1/N) \Sigma_{i=1,N} \tau_{ie}$ over the N residues were categorized as short, and the predicted effective correlation times were set to $\tilde{\tau}_{ie}$. For the remaining residues, the predicted effective correlation times were τ_{ie}. With this heuristic definition of effective correlation times, one finds a simple proportionality between experimental and predicted values (see Figure 4b), covering the full range of all $\tau_{ie}^{(exp)}$ values.

Interestingly, the experimental effective correlation times obtained by Akke et al.[9] were extracted from relaxation data using a simple model-free approach for most residues. In this case, the internal correlation function of the $\mathbf{u}(N_iH_i^N)$ vectors

Table 3. Comparison between NCR-Predicted Effective Correlation Times τ_{ie} and $\tilde{\tau}_{ie}$ [see Eqs 8 and 10] in *apo*- and *holo*-Calbindin, Based on Their NMR Structures

	τ_{ie} (eq 8)		$\tilde{\tau}_{ie}$ (eq 10)	
	ρ_l	ρ_s	ρ_l	ρ_s
apo-cabindin	0.57 ± 0.10	0.65 ± 0.05	0.61 ± 0.09	0.61 ± 0.04
holo-calbindin	0.68 ± 0.12	0.55 ± 0.06	0.69 ± 0.12	0.45 ± 0.05

has the functional form given by eq 9. However, for some residues (marked by stars in Figure 4b), an extended model-free (EMF) approach[26] was required. In this case, internal dynamics occur on both fast and slow timescales τ_f and τ_s, associated with distinct order parameters S_f^2 and S_s^2. If $\tau_f \ll \tau_s$, the internal correlation function is monoexponential

$$C_I(t) = S^2 + (S_f^2 - S^2)\, e^{-t/\tau_s} \tag{12}$$

and it is possible to extract τ_s, S_s, and S_f. In the case of *apo*-calbindin, residues which required an analysis of relaxation data by this EMF approach are located in the linker and in the loop II EF-hand, i.e., in regions with slower internal mobility.[9] Interestingly, the NCR model was able to approximately reproduce the profiles of the effective correlation times extracted from experimental data, even for residues where the EMF level of analysis was required (see Figure 4b). This suggests that effective correlation times based on a single NCR model may cover both situations, without additional adjustable parameters.

Predictions for *holo*-Calbindin

Order Parameters. The same strategy was implemented in the case of *holo*-calbindin to investigate the effects of Ca^{2+} binding on the predictions of the internal dynamics of the protein. Binding to Ca^{2+} ions strongly alters the dynamics of the loop II region of calbindin.[9] Indeed, order parameters $S_{ii}^{2(exp)}$ obtained from NMR relaxation measurements show a significant reduction of backbone motions in the *EF*-hand loop regions upon Ca^{2+} binding. In an attempt to predict these effects, the NCR composed of $\mathbf{u}(N_iH_i^N)$ and $\mathbf{u}(C'_iO_i)$ vectors was supplemented with $\mathbf{u}(CaO_i)$ vectors corresponding to the $Ca-O$ bonds formed in the complex. As a test of the efficiency of this strategy, order parameters S_{ii}^2 were predicted for NCRs with and without $\mathbf{u}(CaO_i)$ vectors, based on the NMR structure of *holo*-calbindin. The results are depicted in Figure 5: as expected, the insertion of the $\mathbf{u}(CaO_i)$ vectors into the network affects the predicted dynamics of the protein in the neighborhood of the Ca^{2+} ions. Binding to Ca^{2+} ions clearly induces a higher rigidity, as attested by an increase of the order parameters $S_{ii}^{2(pred)}$ in both calcium-binding loops. Thus, adding $\mathbf{u}(CaO_i)$ vectors to the network significantly improves the agreement between predicted and experimentally derived order parameters $S_{ii}^{2(exp)}$ in *holo*-calbindin. The linear correlation coefficient between predicted and experimental order parameters increases from $\rho_l = 0.61 \pm 0.14$ to $\rho_l = 0.71 \pm 0.13$ upon supplementing the NCR with $\mathbf{u}(CaO_i)$ vectors (see Table 2).

The effects of including the $\mathbf{u}(CaO_i)$ vectors are summarized in Figure 6a, where predicted and experimental order parameters S_{ii}^2 are compared for all residues (see also the correlation plot in Figure 3). Comparison between experimental data and

(26) Clore, G. M.; Szabo, A.; Bax, A.; Kay, L. E.; Driscoll, P. C.; Gronenborn, A. M. *J. Am. Chem. Soc.* **1990**, *112*, 4989.
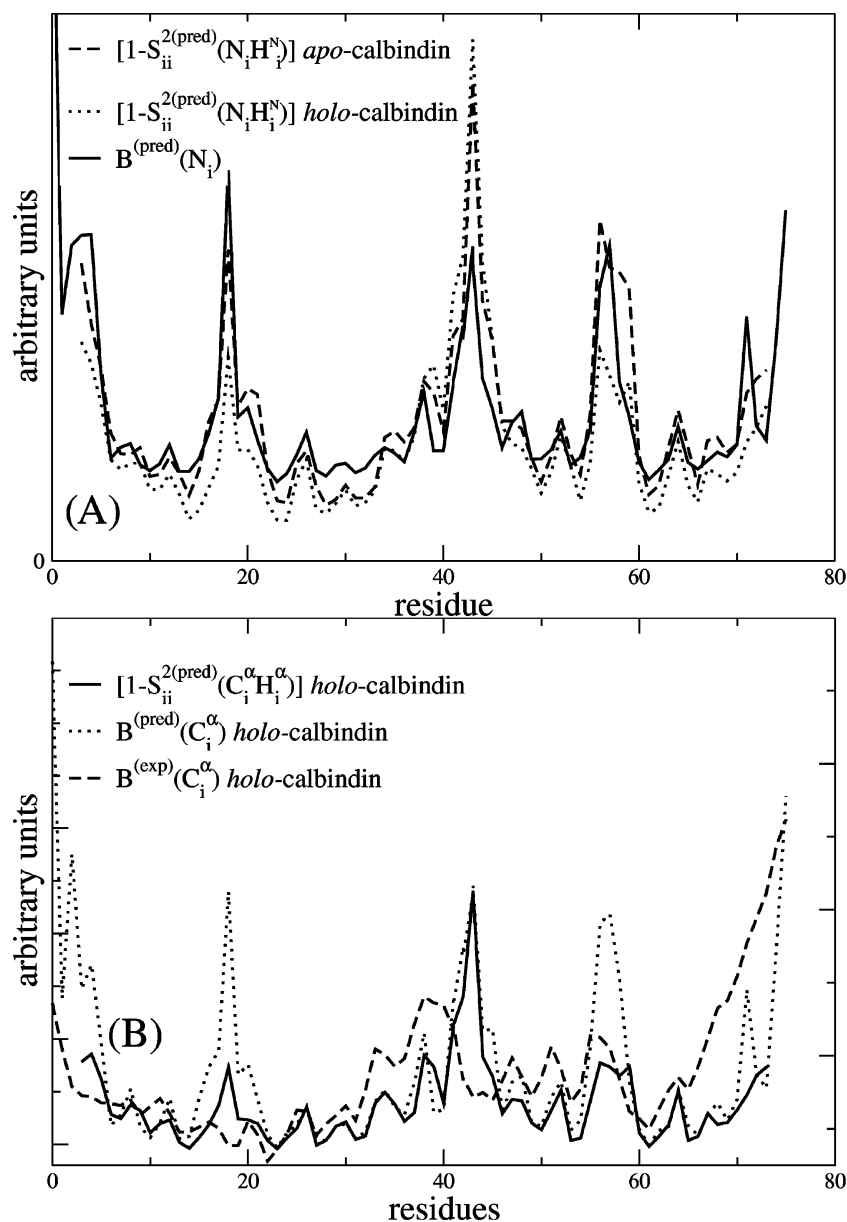
Figure 7. (A) Solid line: $B(N_i)$-factors of the amide N atoms obtained from a Normal Mode Analysis (NMA) based on the Elastic Network Model (ENM) of a "fictitious" structure of *apo*-calbindin obtained by removing the Ca^{2+} ions from the X-ray structure of *holo*-calbindin. Order parameters $[1 - S_{ii}^{2(pred)}(N_iH^{N_i})]$ predicted by the NCR model, using two vector types $\mathbf{u}(C'_iO_i)$ and $\mathbf{u}(N_iH_i^{N})$ and the same structures of *apo*- and *holo*-calbindin (dashed and dotted lines, respectively). (B) Dashed line: experimental $B(C^\alpha_i)$-factors of the C^α atoms in *holo*-calbindin. Dotted lines: $B(C^\alpha)$-factors of the C^α atoms obtained from an NMA analysis based on the X-ray structure. Solid line: order parameters $[1 - S_{ii}^{2(pred)}(C^\alpha_iH^\alpha_i)]$ predicted by NCR for *holo*-calbindin using three vector types $\mathbf{u}(C'_iO_i)$, $\mathbf{u}(N_iH_i^{N})$, and $\mathbf{u}(C_i^\alpha H_i^\alpha)$ with $\kappa_0 = 2$ and $R_c^{max} = 7.5$ Å.

predictions based on the NMR structure of *holo*-calbindin yields $\rho_l = 0.71 \pm 0.13$ and $\rho_s = 0.48 \pm 0.03$ for the linear and rank-order Spearman coefficients. These coefficients take the values $\rho_l = 0.81$ and $\rho_s = 0.52$ when the predictions are based on the X-ray structure of calbindin. It is worth noting that the linear correlation coefficient does not vary much ($\rho_l \approx 0.7$) between the *apo*- and *holo*-forms, whereas the rank-order correlation coefficient ρ_s is markedly lower in *holo*-calbindin. The large difference of ρ_s can be understood by noting that the $S_{ii}^{2(pred)}$ in the loop II region is not completely uniform in the *holo* case but still shows a (significantly attenuated) dip, which does not appear in the experimental profiles (see Figures 4a and 6a). The rank-order correlation coefficient therefore decreases. However, the linear correlation remains strong, owing to the fact that predicted values remain close to the experimental ones. This

observation suggests that there is some scope for further improvement of the model. For example, the predictions might be improved by taking into account the effect of water molecules in exposed areas.

Effective Local Correlation Times. The effective correlation times were predicted for *holo*-calbindin with the two alternative definitions of eqs 8 and 10, like those for *apo*-calbindin. The correlation coefficients between predicted and experimental[9,10] τ_{ie} are $\rho_l = 0.68 \pm 0.12$ and $\rho_s = 0.55 \pm 0.06$. In addition, comparable correlations between predicted $\tilde{\tau}_{ie}$ and $\tau_{ie}^{(exp)}$ were obtained: $\rho_l = 0.69 \pm 0.12$ and $\rho_s = 0.45 \pm 0.05$ (see Table 3). This confirms that effective correlation times calculated by either definition have very similar profiles. The heuristic selection strategy introduced above was used to obtain a compromise set of predicted $\tau_{ie}^{(heur)}$ values. The results are

Table 4. Linear Correlation Coefficients between $B(C_i^\alpha)$- and $B(N_i)$-Factors and NCR-Predicted Order Parameters $S_{ii}^{2(pred)}$ for Various Internuclear Vectors in *holo*- and *apo*-Calbindin, Based on Their NMR Structures

	holo-calbindin			*apo*-calbindin		
	$S^2(C^\alpha H^\alpha)$	$S^2(C'O)$	$S^2(NH)$	$S^2(C^\alpha H^\alpha)$	$S^2(C'O)$	$S^2(NH)$
$B(C_i^\alpha)$-factors	−0.85	−0.81	−0.80	−0.88	−0.87	−0.84
$B(N_i)$-factors			−0.83			−0.83

collected in Figure 6b and clearly show the improvement of the predicted effective correlation times $\tau_{ie}^{(heur)}$ over either of the methods of eq 8 or 10. Interestingly, as noted in *apo*-calbindin, the NCR model is able to reproduce correlation times even for residues that require an extended model-free analysis of the experimental relaxation measurements.

Comparison with *B*-Factors

One way of assessing internal protein mobility consists in determining atomic mean square deviations (AMSDs), denoted $\langle\Delta\mathbf{R}^2\rangle$ where $\Delta\mathbf{R} = \mathbf{R} - \langle\mathbf{R}\rangle$ is the displacement vector of a given atom, which can be obtained experimentally from X-ray diffraction. The *B*-factor is proportional to $\langle\Delta\mathbf{R}^2\rangle$:

$$B = (8\pi^2/3)\langle\Delta\mathbf{R}^2\rangle \tag{11}$$

Our NCR approach provides an alternative description of internal protein dynamics that is adapted to NMR studies, where relaxation rates are related to molecular motions through fluctuations of dipolar and chemical shift anisotropy interactions, rather than to atomic displacements from equilibrium positions. The *B*-factors of C^α and amide N atoms were obtained from a normal-mode analysis (NMA)[2] using the Elastic Network Model (ENM) based on a simple Hookean potential.[3,27] Calculations were made using the ElNémo Web interface.[28] The *B*-factors obtained by NMA computations for amide N atoms in the X-ray structure of *holo*-calbindin are depicted in Figure 7a, together with values $(1 - S_{ii}^{2(exp)})$ determined by ^{15}N relaxation. In order to compare NCR-predicted $[1 - S_{ii}^{2(pred)}(C_i^\alpha H_i^\alpha)]$ with *B*-factors of C_i^α atoms, which are commonly reported in protein studies, we incorporated $\mathbf{u}(C_i^\alpha H_i^\alpha)$ vectors into our network, in addition to $\mathbf{u}(N_i H_i^N)$ and $\mathbf{u}(C'_i O_i)$ vectors. The values of the parameters in the potential of eq 1 were modified accordingly ($\kappa_0 = 2$, $R_c^{max} = 7.5$ Å). Correlation coefficients between *B*-factors for C_i^α atoms and order parameters $[1 - S_{ii}^{2(pred)}(C_i^\alpha H_i^\alpha)]$ are given in Table 4 for both *apo*- and *holo*-calbindin. These calculations show strong correlations between the mobility of backbone atoms and $\mathbf{u}(C'_i O_i)$, $\mathbf{u}(C_i^\alpha H_i^\alpha)$, and $\mathbf{u}(N_i H_i^N)$ vectors ($\rho_l > 0.80$,

see Table 4). This can be related to the fact that although the Elastic Network Model (ENM) and NCR models are very different, they both rely on harmonic potentials, with an energy minimum for the equilibrium structure of the protein. Obviously, there is no formal relationship between *B*-factors and order parameters S_{ii}^2 predicted by our NCR approach, since vector orientations are not directly related to atomic displacements. It is however possible to derive order parameters S_{ii}^2 from the ENM approach, although at the expense of more or less unwarranted geometrical assumptions.[8,29]

In Figure 7b, the NCR-predicted order parameters $[1 - S_{ii}^{2(pred)}(C^\alpha H^\alpha)]$ are compared with those of NMA-predicted and experimental[11] $B(C_i^\alpha)$-factors in *holo*-calbindin. This graph clearly illustrates that, despite local discrepancies, both NMA- and NCR-based predictions yield analogous dynamical pictures of the protein, as indicated by very similar profiles. The agreement between predicted and experimental *B*-factors is not satisfactory in the linker region, where the experimental *B*-factors may reflect static disorder (crystal defects), rather than dynamical effects. It is nevertheless clear from Figure 7b that the correlations of experimental *B*-factors in both Ca^{2+}-binding loop regions (residues 16−24 and 54−62) are more satisfactory with the NCR-predicted order parameters $[1 - S_{ii}^{2(pred)}(C_i^\alpha H_i^\alpha)]$ than with the NMA-predicted *B*-factors. This can easily be understood by noting that the two binding Ca^{2+} ions are not explicitly considered in the Elastic Network Model.[28] In contrast, $Ca−O$ bonds formed upon Ca^{2+} binding are explicitly introduced as vectors in our NCR approach, which therefore takes Ca^{2+} binding into account in a natural and straightforward manner.

Conclusions

In this paper, we have presented a detailed analysis of the internal dynamics of both the *apo*- and *holo*-forms of the calcium-binding protein calbindin, using the networks of coupled rotators (NCRs) introduced recently. It was demonstrated that incorporation into the NCR model of $\mathbf{u}(CaO_i)$ vectors representing the weak interactions between Ca^{2+} ions and oxygen atoms in the binding pockets allowed us to predict variations of order parameters and effective internal correlation times along the backbone. The application of the NCR model to the *apo*/*holo*-calbindin system illustrates the versatility of our approach and suggests that it is applicable to a wide range of systems. Moreover, a new heuristic strategy for the prediction of internal correlation times was introduced, improving the agreement with experiment. Further developments of the methodology, which include the prediction of side-chain dynamics, are under way.

(27) Tama, F.; Sanejouand, Y. H. *Proteins: Struct., Funct., Genet.* **2000**, *41*, 1.
(28) Suhre, K.; Sanejouand, Y. H. *Nucleic Acids Res.* **2004**, *32*, 610.

(29) Sunada, S.; Go, N.; Koehl, P. *J. Chem. Phys.* **1996**, *104*, 4768.